arXiv:1404.6895v3 [nucl-th] 6 Nov 2014

Roles of chiral three-nucleon forces in nucleon-nucleus scattering

Masakazu Toyokawa,[1,*] Kosho Minomo,[2] Michio Kohno,[2,3] and Masanobu Yahiro[1]

[1]*Department of Physics, Kyushu University, Fukuoka 812-8581, Japan*

[2]*Research Center for Nuclear Physics (RCNP), Osaka University, Ibaraki 567-0047, Japan*

[3]*Physics Division, Kyushu Dental University, Kitakyushu 803-8580, Japan*

(Dated: November 7, 2014)

Abstract

We investigate the effects of chiral three-nucleon force (3NF) at NNLO level on nucleon-nucleus (NA) elastic scattering, using the standard framework based on the Brueckner-Hartree-Fock method for nuclear matter and the g-matrix folding model for NA elastic scattering. The optical potential in nuclear matter calculated from chiral two-nucleon force (2NF) at N^{3}LO level is found to be close to that from Bonn-B 2NF, whereas the Melbourne g-matrix is known as a practical effective nucleon-nucleon interaction constructed by localizing the g-matrices calculated from Bonn-B 2NF. As the first attempt to estimate chiral-3NF effects on NA scattering, the effects are simply introduced by multiplying the local Melbourne g-matrix by the ratio of the optical potential in nuclear matter calculated from chiral 2NF+3NF to that from chiral 2NF. For NA elastic scattering on various targets at 65 MeV, chiral 3NF makes the folding potential less attractive and more absorptive. The novel property for the imaginary part is originated in the enhancement of tensor correlations due to chiral 3NF (mainly the 2π-exchange diagram). The two effects are small for differential cross sections and vector analyzing powers at the forward and middle angles where the experimental data are available. If backward measurements are made, the data will reveal the effects of chiral 3NF.

PACS numbers: 21.30.Fe, 24.10.Ht, 25.40.Cm, 25.40.Dn

*toyokawa@phys.kyushu-u.ac.jp

I. INTRODUCTION

Microscopic understanding of nucleon-nucleus (NA) and nucleus-nucleus (AA) optical potentials is one of the primary goals of nuclear physics. The optical potentials play an important role not only in describing elastic scattering but also in analyzing more complicated reactions, since the potentials are inputs of theoretical calculations such as the distorted-wave Born approximation and the continuum discretized coupled-channels method [1–3] for inelastic scattering and transfer and breakup reactions.

NA elastic scattering is less absorptive and hence more transparent than AA elastic scattering. In this sense, NA elastic scattering is more informative. From a theoretical viewpoint based on the multiple scattering theory [4–6], furthermore, the multiple nucleon-nucleon (NN) collision series is much simpler in NA scattering [4, 5] than in AA scattering [6]. Microscopic understanding is thus easier for NA scattering than for AA scattering. In this paper, we focus our discussion on NA scattering.

The g-matrix folding model is a useful tool of describing NA scattering [7–15]. In the model, the optical potential is obtained by folding the g-matrix interaction with the target density. Since the g-matrix is evaluated in nuclear matter, the local-density approximation is taken in the folding procedure. Target-excitation and Pauli-blocking effects are included within the approximation. Among various kinds of g-matrix interactions, the Melbourne g-matrix is successful in reproducing the experimental data on cross sections and spin observables systematically without introducing any ad hoc phenomenological adjustment [14]. This is a monumental achievement in nuclear reaction studies.

The microscopic optical potential calculated with the g-matrix folding model is nonlocal and hence not practical in many applications, but it can be localized with the Brieva-Rook approximation [9]. The validity of the approximation is shown in a wide range of incident energies [16]. The local version of the Melbourne g-matrix folding potential is consistent with the phenomenological optical potentials [17].

Another important issue in nuclear physics is to clarify the roles of three-nucleon force (3NF) in finite nuclei, nuclear reactions and nuclear matter. The phenomenological approach to this issue began with the 2π-exchange 3NF proposed by Fujita and Miyazawa [18]. Attractive 3NFs were introduced to reproduce the binding energies for light nuclei [19], whereas repulsive 3NFs were used to explain the empirical saturation properties in symmetric nuclear matter [20–23]. Recently,

chiral effective field theory (Ch-EFT) made a theoretical breakthrough in this issue [24, 25]. The theory provides a systematic low momentum expansion based on chiral perturbation theory to interactions among nucleons. This allows us to define two-nucleon force (2NF) and 3NF definitely. The roles of chiral 3NF are investigated, for example, in Refs [26–31] for light nuclei and in Refs. [32–35] for nuclear matter. The g-matrix calculated with the Brueckner-Hartree-Fock (BHF) method from chiral 2NF+3NF is successful in reproducing the empirical equation of state (EoS) of symmetric nuclear matter [32–35]. In the framework, the effects of chiral 3NF appear through density (ρ) dependence of the g-matrix.

The effects of 3NF on NA elastic scattering were investigated with CEG07 g-matrix [15] that is constructed from 2NF based on the Nijmegen extended soft-core model [36, 37]. The effects of 3NF are effectively taken into account by introducing the ρ-dependent vector-meson mass that reproduces the empirical EoS. Very recently, the effects of 3NF on NA scattering were investigated [38] with the g-matrix calculated from AV18 2NF [39] plus phenomenological 3NFs [40–42]. The 3NF improves the agreement with measured vector analyzing powers. In these approaches, however, the real and/or imaginary parts of the folding potential are adjusted to measured cross sections.

In this paper, we investigate the roles of chiral 3NF in NA elastic scattering. For this purpose, nuclear matter calculations are done for positive energy (E) by using chiral N^{3}LO 2NF including NNLO 3NF with the cutoff of 550 MeV [43, 44] that well reproduces empirical saturation properties of symmetric nuclear matter for negative E [33, 35]. Even for 2NF, it is quite difficult to treat three-nucleon correlations in nuclear matter calculations. Hence we make the mean-field approximation, that is, we derive an effective 2NF from 3NF by averaging it over the third nucleon in the Fermi sea. The approximation is considered to be good for nucleon elastic scattering in nuclear matter, since nucleons in the Fermi sea are not excited in the final stage of the scattering. The optical (single-particle) potential for the scattering is then calculated from the sum of original and reduced 2NFs by using the BHF method.

The effects of chiral 3NF can be described by the ratio f of the single-particle potential $\mathcal{U}_{(\mathrm{2NF+3NF})}$ calculated from chiral 2NF+3NF to the potential $\mathcal{U}_{(\mathrm{2NF})}$ from chiral 2NF. The single-particle potential is nothing but the optical potential in nuclear matter. The potential $\mathcal{U}_{(\mathrm{2NF})}$ is found to be close to the single-particle potential calculated from Bonn-B 2NF [45], whereas the Melbourne g-matrix is known as a local effective NN interaction obtained by localizing the g-matrices calculated from Bonn-B 2NF [14]. We then simply incorporate the chiral-3NF effects in

the local Melbourne g-matrix by multiplying the g-matrix by the factor f, as the first attempt to estimate the effects on NA scattering. The chiral-3NF effects are investigated at a lower incident energy of $E = 65$ MeV over various targets, since Ch-EFT is more appropriate for lower E.

In Sec. II, we recapitulate the BHF method for the symmetric nuclear matter with both 2NF and 3NF and the g-matrix folding model for the NA system. The modified Melbourne g-matrix with chiral-3NF corrections is also presented. In Sec. III, the results of the g-matrix folding model are shown for NA scattering. Section IV is devoted to a summary.

II. THEORETICAL FRAMEWORK

A. g-matrix calculations for 3NF

We recapitulate the BHF method for nuclear matter with 2NF plus 3NF, following Refs. [33, 35]. It is quite difficult to treat 3NF V_{123} in infinite matter. We then derive an effective 2NF $V_{12(3)}$ from chiral 3NF, using the mean-field approximation [41, 46–48], that is, V_{123} is averaged over the third nucleon in the Fermi sea:

$$\langle \boldsymbol{k}_1', \boldsymbol{k}_2' | V_{12(3)} | \boldsymbol{k}_1, \boldsymbol{k}_2 \rangle_A \equiv \sum_{\boldsymbol{k}_3} \langle \boldsymbol{k}_1', \boldsymbol{k}_2', \boldsymbol{k}_3 | V_{123} | \boldsymbol{k}_1, \boldsymbol{k}_2, \boldsymbol{k}_3 \rangle_A, \tag{1}$$

where the suffix A denotes the antisymmetrization and the symbol $\boldsymbol{k}_i$ stands for quantum numbers (momentum and z components of spin and isospin) of the ith nucleon.

The potential energy is evaluated as

$$\begin{aligned} &\frac{1}{2} \sum_{\boldsymbol{k}_1 \boldsymbol{k}_2} \langle \boldsymbol{k}_1 \boldsymbol{k}_2 | V_{12} | \boldsymbol{k}_1 \boldsymbol{k}_2 \rangle_A + \frac{1}{3!} \sum_{\boldsymbol{k}_1 \boldsymbol{k}_2 \boldsymbol{k}_3} \langle \boldsymbol{k}_1 \boldsymbol{k}_2 \boldsymbol{k}_3 | V_{123} | \boldsymbol{k}_1 \boldsymbol{k}_2 \boldsymbol{k}_3 \rangle_A \\ &= \frac{1}{2} \sum_{\boldsymbol{k}_1 \boldsymbol{k}_2} \langle \boldsymbol{k}_1 \boldsymbol{k}_2 | V_{12} + \frac{1}{3} V_{12(3)} | \boldsymbol{k}_1 \boldsymbol{k}_2 \rangle_A. \end{aligned} \tag{2}$$

This means that the g-matrix g_{12} should be calculated by

$$g_{12} = V_{12}^{\rm eff} + V_{12}^{\rm eff} G_0 g_{12} \tag{3}$$

with the effective 2NF

$$V_{12}^{\rm eff} = V_{12} + \frac{1}{3} V_{12(3)} \tag{4}$$

and the nucleon propagator

$$G_0 = \frac{Q}{E - H}, \tag{5}$$

where Q stands for the Pauli exclusion operator. The g-matrix equation (3) is solved by taking the following continuous prescription for intermediate states. In Eq. (3) for the component $g_{12}|\boldsymbol{k}_1\boldsymbol{k}_2\rangle$, the nucleon propagator is described for intermediate nucleons with momenta $\boldsymbol{k}'_1$ and $\boldsymbol{k}'_2$ as

$$\frac{1}{E-H}|\boldsymbol{k}'_1\boldsymbol{k}'_2\rangle = \frac{1}{e_{\boldsymbol{k}_1}+e_{\boldsymbol{k}_2}-e_{\boldsymbol{k}'_1}-e_{\boldsymbol{k}'_2}}. \tag{6}$$

Here the single-particle energy $e_{\boldsymbol{k}}$ for nucleon with momentum $\boldsymbol{k}$ is defined by

$$e_{\boldsymbol{k}} = \langle \boldsymbol{k}|t|\boldsymbol{k}\rangle + \mathrm{Re}[\mathcal{U}(\boldsymbol{k})], \tag{7}$$

where t denotes the kinetic-energy operator of nucleon and $\mathcal{U}$ stands for the single-particle potential defined by [35]

$$\mathcal{U}(\boldsymbol{k}) = \sum_{\boldsymbol{k}'}^{k_{\mathrm{F}}} \langle \boldsymbol{k}\boldsymbol{k}'|g_{12} + \frac{1}{6}V_{12(3)}(1+G_0 g_{12})|\boldsymbol{k}\boldsymbol{k}'\rangle_A. \tag{8}$$

The single-particle energy is nothing but the optical potential in nuclear matter. Holt *et al.* evaluated the single-particle potential $\mathcal{U}$ within the framework of Ch-EFT by using the second-order perturbation [49]. Our formulation is consistent with theirs. The factor $1/6$ in Eq. (8) is important for the consistency [33, 35].

In actual calculations, the partial wave expansion [50] is taken with the angle-average approximation to Q. The validity is shown in Ref. [51]. Partial waves up to the total angular momentum $J = 7$ and the orbital angular momentum $\ell = 7$ are taken into account in the calculations. The low-energy constants of chiral interactions are taken from those of the Jülich group [43]: $c_1 = -0.81$ GeV^{-1}, $c_3 = -3.4$ GeV^{-1}, and $c_4 = 3.4$ GeV^{-1}. The other constants are taken from Ref. [44]: $c_D = -4.381$ and $c_E = -1.126$. The original and effective 2NFs, V_{12} and $V_{12(3)}$, are regularized with the common form factor $\exp\{-(q'/\Lambda)^6 - (q/\Lambda)^6\}$ with $\Lambda = 550$ MeV.

There are several different sets of low-energy constants in the literature [28, 52]. The values of these constants are essentially same. In addition, as was shown in Ref. [35], the variation of G-matrices in nuclear matter in the 2NF level is much reduced when the 3NF effects are consistently incorporated. As for the parameters c_D and c_E, the net effect of these terms is small, as far as the relation $c_D \simeq 4c_D$ holds. This relation is actually realized in various calculations in light nuclei [29, 53] and in nuclear matter [44]. The results of BHF calculations do not depend on specific values of c_D and c_E, as far as $c_D \simeq 4c_D$ is held.

The g-matrix thus obtained is a function of the starting energy E and the Fermi momentum k_{F}, and can be classified as $g^{ST}(k_{\mathrm{F}}, E)$ with the total-spin (S) and total-isospin (T) of the NN system.

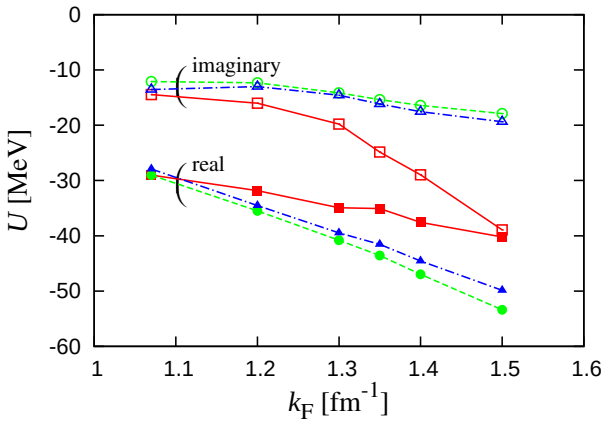

FIG. 1: (Color online) $k_{\rm F}$ dependence of the single-particle potentials $\mathcal{U}$ at $E = 65$ MeV. The squares, circles, and triangles show the results of chiral 2NF+3NF, chiral 2NF and Bonn-B 2NF, respectively. The closed (open) symbols correspond to the real (imaginary) part of single-particle potential.

We can then decompose the single-particle potential $\mathcal{U}$ into

$$\mathcal{U} = \sum_{ST}(2S+1)(2T+1)\mathcal{U}^{ST}, \tag{9}$$

with $\mathcal{U}^{ST}$ obtained from g^{ST} as

$$\mathcal{U}^{ST}(k_{\rm F}, E) = \sum_{\boldsymbol{k}'}^{k_{\rm F}} \langle \boldsymbol{k}\boldsymbol{k}'|g^{ST} + \frac{1}{6}V_{12(3)}^{ST}(1+G_0 g^{ST})|\boldsymbol{k}\boldsymbol{k}'\rangle_A, \tag{10}$$

where $\boldsymbol{k}$ is related to E as $E = (\hbar\boldsymbol{k})^2/(2m) + {\rm Re}[\mathcal{U}]$ for the nucleon mass m. Here $\mathcal{U}^{ST}$ represents the single-particle potential in each spin-isospin channel. For the symmetric nuclear matter where the proton density ρ_p is the same as the neutron one ρ_n, the Fermi momentum $k_{\rm F}$ is related to the matter density $\rho = \rho_p + \rho_n$ as $k_{\rm F}^3 = 3\pi^2\rho/2$ and hence the normal density $\rho = \rho_0 = 0.17$ fm^{-3} corresponds to $k_{\rm F} = 1.35$ fm^{-1}. On the right hand side of Eq. (10), the second term is ten times as small as the first term at the normal density. In the first term as the main component, the potential $\mathcal{U}^{ST}$ is determined from the on-shell component of g^{ST}.

Figure 1 shows $k_{\rm F}$ dependence of the single-particle potential $\mathcal{U}$ at $E = 65$ MeV. The squares, circles, and triangles denote the results of chiral 2NF+3NF, chiral 2NF and Bonn-B 2NF, respectively. The effects of chiral 3NF are shown by the difference between squares and circles. The difference mainly comes from the 2π-exchange 3NF shown by diagram (a) in Fig. 2. The effects become significant in the region $k_{\rm F} \gtrsim 1.2$ fm^{-1}. Particularly for NA scattering, the chiral-3NF

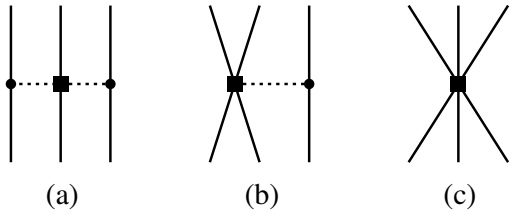

FIG. 2: Diagrams for NNLO 3NF. The solid and dashed lines are nucleon and pion propagations, respectively. Diagrams (a), (b), and (c) correspond to the 2π-exchange, the 1π-exchange, and the contact interactions.

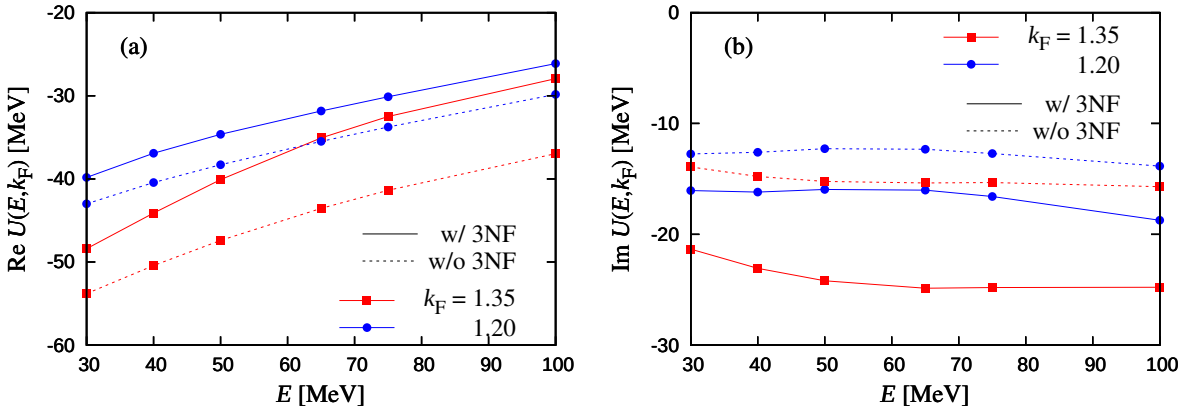

FIG. 3: (Color online) E dependence of the single-particle potentials $\mathcal{U}$ at $k_{\rm F} = 1.35$ fm^{-1} ($\rho = \rho_0$) and $k_{\rm F} = 1.2$ fm^{-1} ($\rho = 0.7\rho_0$). Panels (a) and (b) represent the real and imaginary strength, respectively. The results of chiral 2NF+3NF (chiral 2NF) are denoted by the solid (dashed) lines with symbols. The square (circle) symbols correspond to the results of $k_{\rm F} = 1.35$ fm^{-1} (1.2 fm^{-1}).

effects in the region $1.2 \lesssim k_{\rm F} \lesssim 1.35$ fm^{-1} ($0.7\rho_0 \lesssim \rho \lesssim \rho_0$) affect the scattering. In addition, the result of Bonn-B 2NF (triangles) agrees well with that of chiral 2NF (circles) at $k_{\rm F} < 1.35$ fm^{-1} important for the NA scattering.

Figure 3 shows $\mathcal{U}$ as a function of E for $k_{\rm F} = 1.35$ fm^{-1} ($\rho = \rho_0$) and $k_{\rm F} = 1.2$ fm^{-1} ($\rho = 0.7\rho_0$). At low E such as $0 < E \lesssim 20$ MeV, the g-matrix in nuclear matter may not describe in-medium effects in finite nuclei accurately, since the energy levels are discrete in finite nuclei but continuous in nuclear matter. We then take the energy range $30 < E < 100$ MeV in Fig. 3. Chiral-3NF effects are shown by the difference between the solid line and the corresponding dashed line.

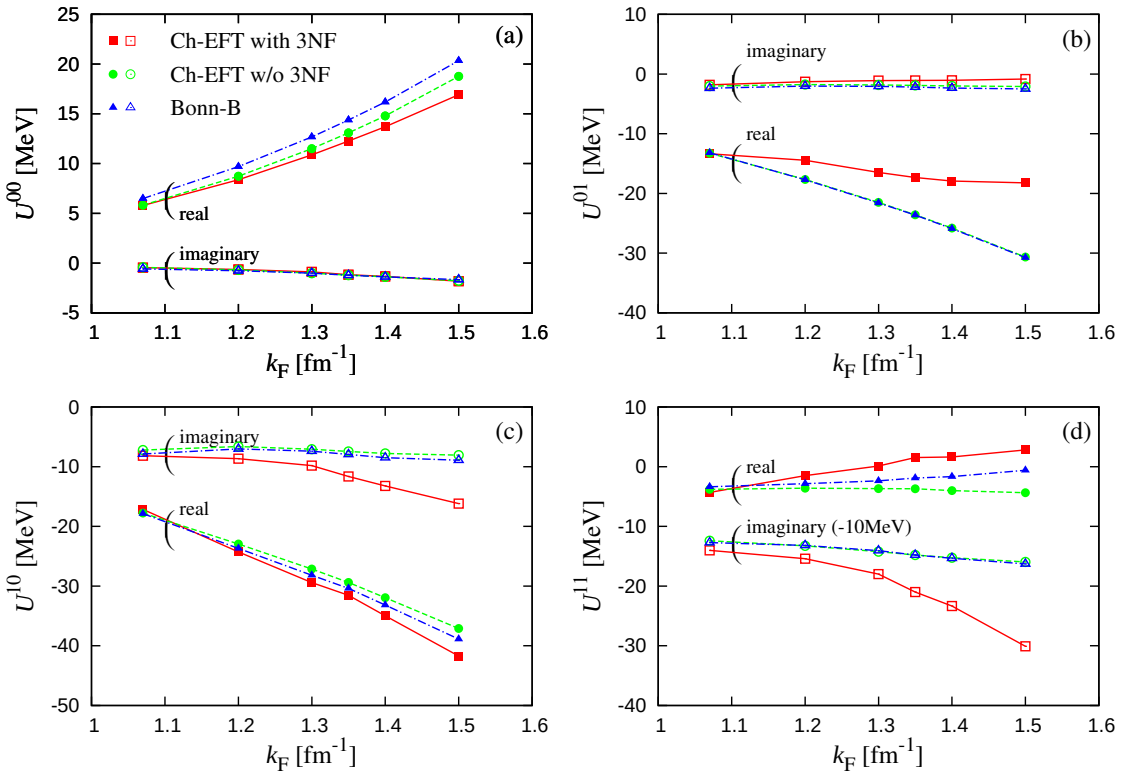

FIG. 4: (Color online) $k_{\rm F}$ dependence of $\mathcal{U}^{ST}$ at $E = 65$ MeV for (a) ^{1}O, (b) ^{1}E, (c) ^{3}E, and (d) ^{3}O channel. The squares, circles, and triangles show the results of chiral 2NF+3NF, chiral 2NF and Bonn-B 2NF, respectively. The closed (open) symbols correspond to the real (imaginary) part of single-particle potential. For ^{3}O, the imaginary part is shifted down by 10 MeV.

The effects are significant in the energy range for both cases of $k_{\rm F} = 1.35$ and 1.2 fm^{-1}, although the effects become small as $k_{\rm F}$ decreases.

The single-particle potential within the framework of Ch-EFT is also presented by Holt *et al*. [49] in the second-order perturbation. It is interesting to compare our single-particle potentials with those of Holt *et al.* (Figs. 8 and 9 of Ref. [49]). In the case of $\rho = \rho_0$, their potential is similar to ours for the real strength. For the imaginary strength, meanwhile, our case is more absorptive than that of Holt *et al.* in the range $30 < E < 100$ MeV. For example, it differs by a factor of about 2 at $E = 65$ MeV. This may be due to the full ladder-summation in our g-matrix calculation.

Now we decompose $\mathcal{U}$ into the $\mathcal{U}^{ST}$ to see the detail of chiral-3NF effects in Fig. 4. Again, the squares, circles, and triangles correspond to the results of chiral 2NF+3NF, chiral 2NF and Bonn-B 2NF, respectively. Here we represent the channels of the NN system as $^{2S+1}\mathcal{P}$ with the

parity $\mathcal{P}$ and the spin multiplicity $(2S+1)$; hence, ^{1}E, ^{3}E, ^{1}O, ^{3}O channels correspond to $(S,T) = (0,1),(1,0),(0,0),(1,1)$ channels, respectively. For the triplet (^{3}E and ^{3}O) channels, the 2π-exchange 3NF enhances tensor correlations and hence couplings between different states. This makes the imaginary part of $\mathcal{U}^{ST}$ more absorptive. For the real part, the stronger tensor correlations make $\mathcal{U}^{ST}$ more attractive for ^{3}E and less attractive for ^{3}O. For the ^{1}E channel, the contribution of the 2π-exchange 3NF corresponds to suppressing transitions to Δ resonance due to Pauli blocking, and consequently makes $\mathcal{U}^{ST}$ less attractive.

The $\mathcal{U}^{ST}$ calculated from chiral 2NF (circles) is close to that from Bonn-B 2NF (triangles) except for the real part of $\mathcal{U}^{ST}$ in the odd (^{1}O and ^{3}O) channels. However, the deviation is not important, because the odd components hardly contribute to the folding potential for NA scattering as mentioned later below Eq. (22). In general, the g-matrix is nonlocal and hence not practical. For this reason, the g-matrix is usually presented by assuming a local form such as Gaussian and Yukawa functions. The Melbourne group has already constructed a local effective interaction on the basis of the nonlocal g-matrices calculated from Bonn-B 2NF [14]. We then introduce the effects of chiral 3NF by multiplying the central part $g^{ST}(\boldsymbol{s}; k_{\rm F}, E)$ of the local Melbourne g-matrix by the factor

$$f^{ST}(k_{\rm F}, E) = \mathcal{U}^{ST}_{(\rm 2NF+3NF)}(k_{\rm F}, E)/\mathcal{U}^{ST}_{(\rm 2NF)}(k_{\rm F}, E), \tag{11}$$

where the argument $\boldsymbol{s}$ in $g^{ST}(\boldsymbol{s}; k_{\rm F}, E)$ denotes the coordinate between two correlated nucleons and $\mathcal{U}^{ST}_{(\rm 2NF+3NF)}(k_{\rm F}, E)$ and $\mathcal{U}^{ST}_{(\rm 2NF)}(k_{\rm F}, E)$ are the single-particle potentials with and without chiral-3NF effects, respectively. The present prescription is then described by

$$g^{ST}(\boldsymbol{s}; k_{\rm F}, E) \to f^{ST}(k_{\rm F}, E) g^{ST}(\boldsymbol{s}; k_{\rm F}, E). \tag{12}$$

As mentioned above, the factor f^{ST} is mainly determined from the on-shell component of the g-matrix. However, it should be noted that when $V_{123} \neq 0$, the off-shell component of the g-matrix contributes to the factor f^{ST} through the second term of Eq. (10).

It is shown in Ref. [33] that the spin-orbit part of the g-matrix is enhanced by chiral 3NF at most by a factor of 4/3. This effect is also simply estimated by multiplying the spin-orbit part of the Melbourne g-matrix by the factor, since the effect is small for the present NA scattering.

B. Folding model

We recapitulate the folding model, following Ref. [17]. Since the formalism is parallel between proton and neutron scattering, we mainly consider proton scattering as an example. Proton elastic scattering can be described as a one-body scattering distorted by an optical potential U:

$$(T_{\boldsymbol{R}} + U - E)\Psi^{(+)} = 0, \tag{13}$$

where E denotes the energy of an incident proton and $T_{\boldsymbol{R}}$ stands for the kinetic energy with respect to the relative coordinate $\boldsymbol{R}$ between an incident proton and a target (T). The optical potential U can be divided into the central (CE), the spin-orbit (LS), and the Coulomb (Coul) component:

$$U = U_{\rm CE} + U_{\rm LS}\boldsymbol{L}\cdot\boldsymbol{\sigma} + V_{\rm Coul}. \tag{14}$$

In the g-matrix folding model, U is obtained by folding the g-matrix with the density of T:

$$U(\boldsymbol{R}) = \langle\Phi_0|\sum_{j\in{\rm T}} g_{pj}|\Phi_0\rangle\ , \tag{15}$$

where Φ_0 is the ground state of T. The resulting potential is composed of the direct and exchange parts: $U = U^{\rm DR} + U^{\rm EX}$. Since the $U^{\rm EX}$ is nonlocal, it is localized with the Brieva-Rook approximation [9]. The validity of this approximation is shown in Ref. [16]. The central part $U_{\rm CE}$ of the localized U is then described as [9, 12, 15]

$$U_{\rm CE} \equiv V_{\rm CE} + iW_{\rm CE} = U^{\rm DR}_{\rm CE} + U^{\rm EX}_{\rm CE} \tag{16}$$

with

$$U^{\rm DR}_{\rm CE}(\boldsymbol{R}) = \sum_{\alpha=p,n}\int\rho_\alpha(\boldsymbol{r})g^{\rm DR}_{p\alpha}(\boldsymbol{s};\rho_\alpha)d\boldsymbol{r}, \tag{17}$$

$$U^{\rm EX}_{\rm CE}(\boldsymbol{R}) = -\sum_{\alpha=p,n}\int\rho_\alpha(\boldsymbol{r},\boldsymbol{r}-\boldsymbol{s})g^{\rm EX}_{p\alpha}(\boldsymbol{s};\rho_\alpha)j_0(Ks)d\boldsymbol{r}, \tag{18}$$

where $\boldsymbol{s} = \boldsymbol{r} - \boldsymbol{R}$ for the coordinate $\boldsymbol{r}$ of an interacting nucleon from the center-of-mass (c.m.) of T, and $V_{\rm CE}$ and $W_{\rm CE}$ are the real and imaginary parts of $U_{\rm CE}$, respectively. Here the mixed density $\rho_\alpha(\boldsymbol{r},\boldsymbol{R})$ is usually calculated with the local Fermi-gas approximation [54]:

$$\rho_\alpha(\boldsymbol{r},\boldsymbol{R}) \approx \rho_\alpha\left(\boldsymbol{r}_m\right) D_\alpha(\tilde{s}) \tag{19}$$

with

$$D_\alpha(\tilde{s}) = \frac{3}{\tilde{s}^3}[\sin(\tilde{s}) - \tilde{s}\cos(\tilde{s})], \tag{20}$$

for $\tilde{s} = sk_{\rm F}^\alpha(r_m)$ and the midpoint $\boldsymbol{r}_m = \boldsymbol{R} + \boldsymbol{s}/2$ between two correlated nucleons, where $k_{\rm F}^\alpha(r_m)$ is related to the local density $\rho_\alpha(r_m)$ as $k_{\rm F}^\alpha(r_m)^3 = 3\pi^2\rho_\alpha(r_m)$. The local momentum $K(R)$ present in Eq. (18) is obtained self-consistently, since it is defined as $\hbar K(R) \equiv \sqrt{2\mu_R(E - U_{\rm CE} - V_{\rm Coul})}$ for the reduced mass μ_R of the projectile+target system.

The direct and exchange parts of the g-matrix interaction, $g_{p\alpha}^{\rm DR}$ and $g_{p\alpha}^{\rm EX}$, are assumed to be a function of the local density $\rho_\alpha = \rho_\alpha(\boldsymbol{r}_m)$ at the midpoint of the interacting nucleon pair. The direct and exchange parts are described by

$$g_{pp}^{\rm DR,EX}(s;\rho_p) = g_{nn}^{\rm DR,EX}(s;\rho_p) = \frac{1}{4}\left(\pm g^{01} + 3g^{11}\right), \tag{21}$$

$$g_{pn}^{\rm DR,EX}(s;\rho_n) = \frac{1}{8}\left(g^{00} \pm g^{01} \pm 3g^{10} + 3g^{11}\right). \tag{22}$$

The even (^{1}E and ^{3}E) components of g^{ST} dominate $U_{\rm CE}$, since the odd (^{1}O and ^{3}O) components are almost canceled each other between $U_{\rm CE}^{\rm DR}$ and $U_{\rm CE}^{\rm EX}$. The same derivation is possible for the spin-orbit part,

$$U_{\rm LS} \equiv V_{\rm LS} + iW_{\rm LS} = U_{\rm LS}^{\rm DR} + U_{\rm LS}^{\rm EX}; \tag{23}$$

see Refs. [15, 17] for the explicit form of $U_{\rm LS}$.

For heavier targets with the mass number A larger than 40, the matter densities are evaluated with spherical Hartree-Fock (HF) calculations with the Gogny-D1S interaction [55] in which the spurious c.m. motions are removed in the standard manner [56]. For lighter targets of $A \leq 40$, the phenomenological proton-density [57] is taken, where the finite-size effect of proton charge is unfolded with the standard procedure [58]. The neutron density is assumed to have the same geometry as the proton one, since the difference between the neutron root-mean-square radius and the proton one is only 1% in spherical HF calculations.

III. RESULTS

Figure 5 shows differential cross sections $d\sigma/d\Omega$ and vector analyzing powers A_y for proton elastic scattering at $E = 65$ MeV on various targets from ^{12}C to ^{208}Pb. The solid (dashed) lines

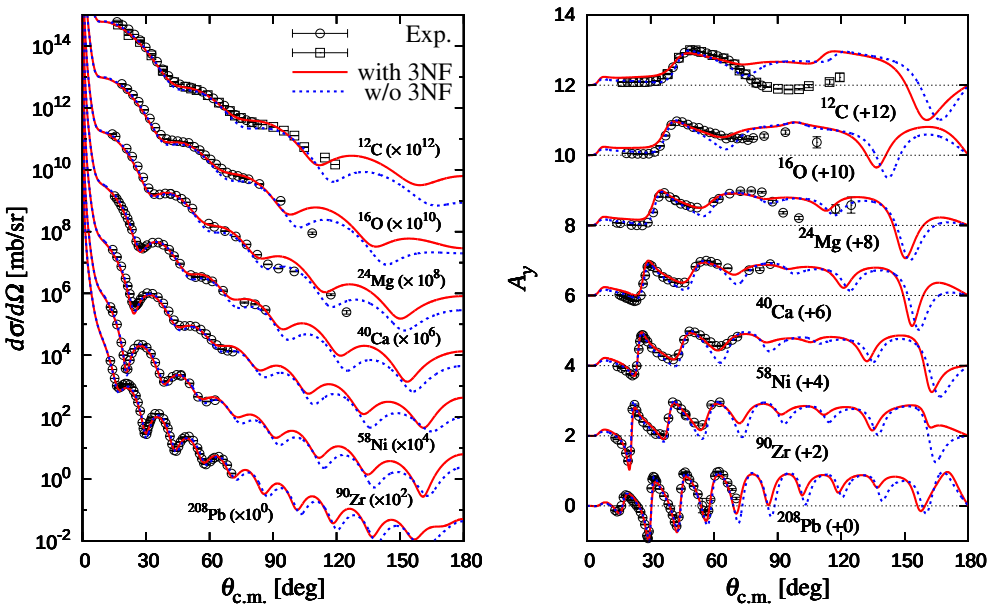

FIG. 5: (Color online) Differential cross sections and vector analyzing powers for proton elastic scattering at 65 MeV. The solid (dashed) curves represent the results of Melbourne g-matrix with (without) chiral-3NF corrections. Each cross section is multiplied by the factor shown in the figure, while each vector analyzing power is shifted up by the number shown in the figure. Experimental data are taken from Ref. [59–62].

stand for the results of Melbourne g-matrix with (without) chiral-3NF corrections. The chiral-3NF effects are small at the forward and middle angles where the experimental data [59–62] are available. Only an exception is A_y around $\theta = 60^\circ$. The chiral-3NF effects improve the agreement with the experimental data there. Similar improvement is also seen in the previous work [38] based on the phenomenological 3NFs. This smallness of chiral-3NF effects comes from the fact that the effects are significant only in $\rho \gtrsim 0.7\rho_0$. The chiral-3NF effects become significant at backward angles, although the experimental data are not available there. The backward measurements are thus important to investigate chiral-3NF effects. Also for neutron scattering at 65 MeV, the chiral-3NF effects are small at forward and middle angles and become significant for backward angles, as shown in Fig. 6.

Figure 7 shows reaction cross sections $\sigma_{\rm R}$ for proton scattering around E=65 MeV on various targets from ^{12}C to ^{208}Pb. In panel (a), the $\sigma_{\rm R}$ are plotted as a function of target mass number A. The circles (triangles) stand for the results of Melbourne g-matrix with (without) chiral-3NF corrections. The effects of chiral 3NF on $\sigma_{\rm R}$ are small, so that both the Melbourne g-matrix and

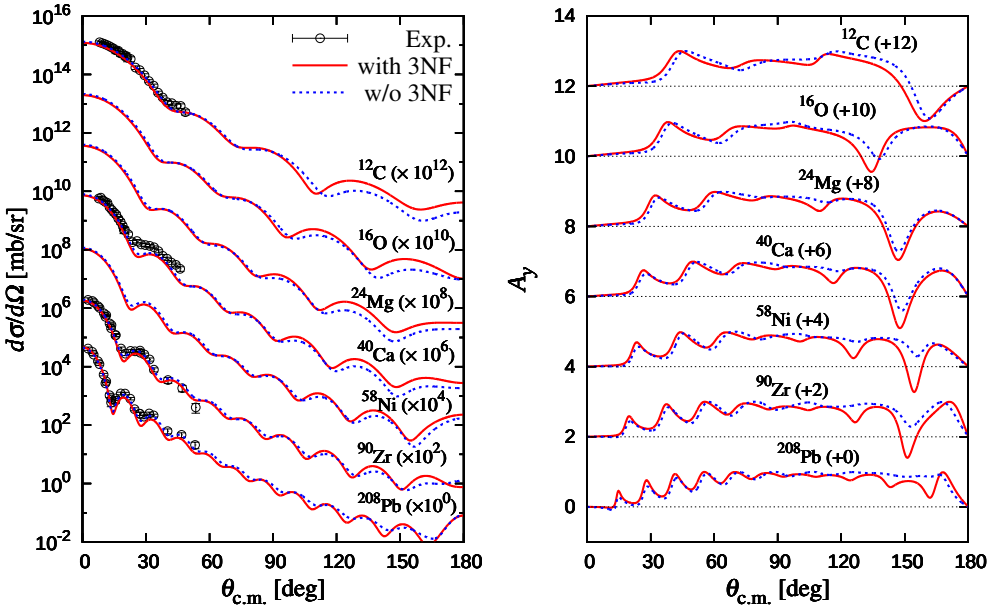

FIG. 6: (Color online) Differential cross sections and vector analyzing powers for neutron elastic scattering at 65 MeV. The solid (dashed) curves represent the results of Melbourne g-matrix with (without) chiral-3NF corrections. Each cross section is multiplied by the factor shown in the figure, while each vector analyzing power is shifted up by the number shown in the figure. Experimental data are taken from Ref. [63, 64].

the modified Melbourne g-matrix with chiral-3NF corrections reproduce the measured $\sigma_{\rm R}$. The agreement of the theoretical results with the experimental data are particularly good for heavier targets such as ^{116}Sn and ^{208}Pb where the local density approximation is considered to be good. In panel (b), the relative difference

$$\delta = \frac{\sigma_{\rm R}^{\rm 2NF+3NF} - \sigma_{\rm R}^{\rm 2NF}}{\sigma_{\rm R}^{\rm 2NF}} \tag{24}$$

is plotted as a function of A. The chiral 3NF enhances $\sigma_{\rm R}$ only by a few percent, so that the Melbourne g-matrix keeps good agreement with the experimental data.

The probability $P(R)$ of elastic scattering at each R can be described by the elastic S-matrix element S_L as $P(R) = |S_L|^2$, where R can be estimated from the relative angular momentum L between proton and T with the semi-classical relation $L = RK(\infty)$. Figure 8 shows $P(R)$ as a function of R for proton scattering from ^{12}C, ^{58}Ni and ^{208}Pb at $E = 65$ MeV. The solid (dashed) lines stand for the results of Melbourne g-matrix with (without) chiral-3NF corrections. The chiral-3NF effects appear mainly in the inner region of T where $P(R)$ is small, and make $P(R)$ even smaller. In Fig. 9, the central part of U is plotted as a function of R for ^{58}Ni. The

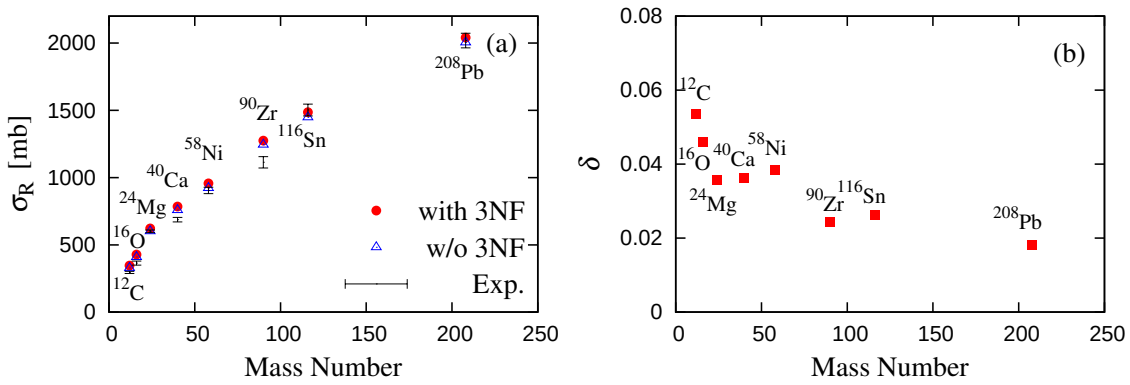

FIG. 7: (Color online) Reaction cross sections $\sigma_{\rm R}$ for proton scattering around $E = 65$ MeV. The theoretical results are compared with the experimental data at $E = 65.5$ MeV for ^{12}C, ^{16}O, ^{40}Ca, ^{58}Ni, ^{116}Sn, ^{208}Pb, 48.0 MeV for ^{24}Mg and 60.8 MeV for ^{90}Zr. In panel (a) the $\sigma_{\rm R}$ are plotted as a function of A. The circles (triangles) denote the results of Melbourne g-matrix with (without) chiral-3NF corrections. In panel (b), the relative difference δ due to chiral 3NF is shown as a function of A. Experimental data are taken from Refs. [65–67].

chiral 3NF makes U more absorptive and less attractive. The effects in the peripheral region of $R \gtrsim 4$ fm affect $d\sigma/d\Omega$ and A_y at the forward and middle angles where the experimental data are available. In the inner region of $R \lesssim 4$ fm, the chiral 3NF little affects $d\sigma/d\Omega$ and A_y at the forward and middle angles, since $P(R)$ is already small in the results of Melbourne g-matrix without chiral-3NF corrections.

In the folding procedure, the even (^{1}E and ^{3}E) components of g^{ST} dominate $U_{\rm CE}$, since the odd (^{1}O and ^{3}O) components are almost canceled each other between $U_{\rm CE}^{\rm DR}$ and $U_{\rm CE}^{\rm EX}$. This means that the repulsive effect of chiral 3NF on $V_{\rm CE}$ comes from the same effect on $\mathcal{U}^{ST}$ in the ^{1}E channel, that is, from the suppression of transitions to Δ resonance due to Pauli blocking. Similarly, the strong absorption effect of chiral 3NF on $W_{\rm CE}$ is originated in the enhancement of tensor correlations due to chiral 3NF.

IV. SUMMARY

We have investigated the roles of chiral NNLO 3NF in NA elastic scattering, using the standard framework based on the BHF method for nuclear matter and the folding model for NA scattering. Ch-EFT is a definite way of organizing interactions among nucleons, and consequently, 2NF and

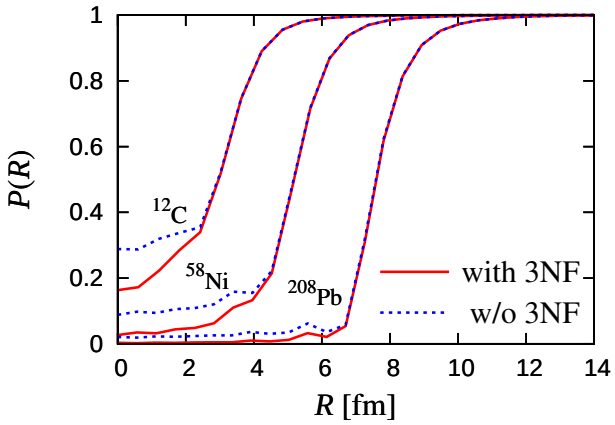

FIG. 8: (Color online) The probability $P(R)$ of elastic scattering as a function of R for proton scattering from ^{12}C, ^{58}Ni and ^{208}Pb at $E = 65$ MeV. The solid (dashed) lines represent the results of Melbourne g-matrix with (without) chiral-3NF corrections.

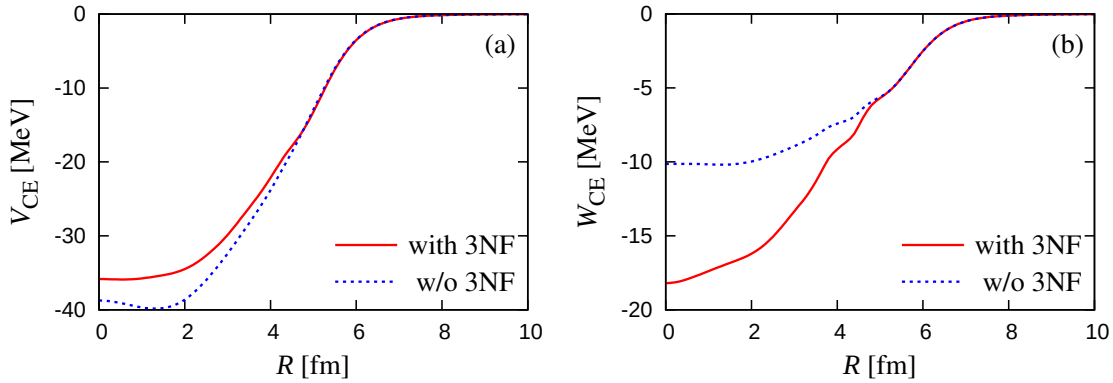

FIG. 9: (Color online) R dependence of the central part of the folding potential for p+^{58}Ni elastic scattering at $E = 65$ MeV. Panels (a) and (b) correspond to the real and imaginary parts, respectively. The solid (dashed) lines represent the results of Melbourne g-matrix with (without) chiral-3NF corrections.

3NF are consistently defined. The present framework based on Ch-EFT has been applied to NA scattering at a lower incident energy of $E = 65$ MeV over various targets, since Ch-EFT is more reliable for lower E.

BHF calculations were done for positive energy with chiral N^{3}LO 2NF including NNLO 3NF with the cutoff Λ of 550 MeV on the basis that the same calculations for negative energies well reproduce empirical saturation properties of symmetric nuclear matter. The single-particle po-

tential calculated from chiral 2NF+3NF deviates from that from chiral 2NF in the density region $\rho \gtrsim 0.7\rho_0$. The difference mainly comes from the 2π-exchange diagram. The diagram generates absorptive corrections in the triplet channels by enhancing tensor correlations and repulsive corrections in the singlet ^{1}E channel by suppressing transitions to Δ resonance due to Pauli blocking. The repulsive contribution in the ^{1}E channel dominates the effects of chiral 3NF on the real part of the g-matrix.

The effects of chiral 3NF are incorporated in the folding potential with the following simple procedure, as the first estimate of chiral-3NF effects on NA scattering. The Melbourne group has already constructed the local effective interaction on the basis of the g-matrices from Bonn-B 2NF. The single-particle potential calculated from chiral 2NF with $\Lambda = 550$ MeV is found to be close to that from Bonn-B 2NF. We have then modified the Melbourne g-matrix so as to reproduce the single-particle potentials obtained from chiral 2NF+3NF. In the procedure, the effects of chiral 3NF on the on-shell component of the g-matrix are approximately taken into account. The chiral-3NF effects are small for differential cross sections and vector analyzing powers at the forward and middle angles where the experimental data are available, but the effects surely improve the agreement with measured vector analyzing powers around middle angles. Similar improvement is also seen in the previous work [38] based on phenomenological 3NFs.

Chiral 3NF, mainly in its the 2π-exchange diagram, makes the folding potential less attractive and more absorptive. In the previous work [38], phenomenological 3NFs make the potential less attractive but less absorptive. Thus, chiral 3NF yields a different property for the imaginary part of the folding potential. This novel property is originated in the enhancement of tensor correlations due to the 2π-exchange diagram. Ch-EFT, furthermore, says that the repulsive effect of the diagram on the folding model comes from the suppression of transitions to Δ resonance due to Pauli blocking.

Owing to the density dependence of 3NF contributions, the chiral-3NF effects are sizable in the inner region of target, but small in the peripheral region. The large effect in the inner region is, however, masked by the strong absorption of the incident flux. Consequently, the chiral-3NF effects are small for NA scattering at the forward and middle angles where the experimental data are available at present. This is the reason why the Melbourne g-matrix with no 3NF effects well accounts for measured cross sections and vector analyzing powers for NA scattering. If the measurements are made at backward angles, the data should reveal chiral-3NF effects. Another possibility of detecting the chiral-3NF effects is in transfer reactions such as (d, p) reactions, since

the optical potential itself changes sizably with the effects. Furthermore, AA scattering is also interesting, since the density higher than $0.7\rho_0$ is certainly realized in the scattering. We discuss this subject in a separate paper [68] by using the double-folding model.

Acknowledgements

This work is supported in part by by Grant-in-Aid for Scientific Research (Nos. 244137, 25400266, and 26400278) from Japan Society for the Promotion of Science (JSPS).

---

[1] M. Kamimura, M. Yahiro, Y. Iseri, Y. Sakuragi, H. Kameyama, and M. Kawai, Prog. Theor. Phys. Suppl. **89**, 1 (1986).

[2] N. Austern, Y. Iseri, M. Kamimura, M. Kawai, G. Rawitscher, and M. Yahiro, Phys. Rep. **154**, 125 (1987).

[3] M. Yahiro, K. Ogata, T. Matsumoto, and K. Minomo, Prog. Theor. Exp. Phys. **2012**, 01A206 (2012).

[4] K. M. Watson, Phys. Rev. **89**, 575 (1953).

[5] A. K. Kerman, H. McManus, and R. M. Thaler, Ann. Phys. **8**, 551 (1959).

[6] M. Yahiro, K. Minomo, K. Ogata, and M. Kawai, Prog. Theor. Phys. **120**, 767 (2008).

[7] G. Bertsch, J. Borysowicz, H. McManus, and W. G. Love, Nucl. Phys. A **284**, 399 (1977).

[8] J. -P. Jeukenne, A. Lejeune, and C. Mahaux, Phys. Rev. C**16**, 80 (1977); J. -P. Jeukenne, A. Lejeune, and C. Mahaux, Phys. Rep. **25**, 83 (1976).

[9] F. A. Brieva and J. R. Rook, Nucl. Phys. A **291**, 299 (1977); *ibid.* **291**, 317 (1977); *ibid.* **297**, 206 (1978).

[10] G. R. Satchler and W. G. Love, Phys. Rep. **55**, 183 (1979).

[11] G. R. Satchler, "Direct Nuclear Reactions", Oxfrod University Press, (1983).

[12] N. Yamaguchi, S. Nagata, and T. Matsuda, Prog. Theor. Phys. **70**, 459 (1983); N. Yamaguchi, S. Nagata, and J. Michiyama, Prog. Theor. Phys. **76**, 1289 (1986).

[13] L. Rikus, K. Nakano, and H. V. Von Geramb, Nucl. Phys. A **414**, 413 (1984); L. Rikus, and H. V. Von Geramb, Nucl. Phys. A **426**, 496 (1984).

[14] K. Amos, P. J. Dortmans, H. V. Von Geramb, S. Karataglidis, and J. Raynal, in *Advances in Nuclear Physics*, edited by J. W. Negele and E. Vogt(Plenum, New York, 2000) Vol. 25, p. 275.

[15] T. Furumoto, Y. Sakuragi, and Y. Yamamoto, Phys. Rev. C **78**, 044610 (2008).

[16] K. Minomo, K. Ogata, M. Kohno, Y. R. Shimizu, and M. Yahiro, J. Phys. G **37**, 085011 (2010) [arXiv:0911.1184 [nucl-th]].

[17] M. Toyokawa, K. Minomo, and M. Yahiro, Phys. Rev. C **88**, 054602 (2013).

[18] J. Fujita and H. Miyazawa, Prog. Theor. Phys. **17**, 360 (1957); *ibid*. **17**, 366 (1957).

[19] R. B. Wiringa and S. C. Pieper, Phys. Rev. Lett. **89**, 182501 (2002).

[20] R. B. Wiringa, V. Fiks, and A. Fabrocini, Phys. Rev. C **38**, 1010 (1988).

[21] H. Müther and A. Polls, Prog. Part. Nucl. Phys. **45**, 243 (2000).

[22] Y. Dewulf, W. H. Dickhoff, D. Van Neck, E. R. Stoddard, and M. Waroquier, Phys. Rev. Lett. **90**, 152501 (2003).

[23] S. K. Bogner, A. Schwenk, R. J. Furnstahl, and A. Nogga, Nucl. Phys. A **763**, 59 (2005).

[24] E. Epelbaum, H.-W. Hammer, and Ulf-G. Meißner, Rev. Mod. Phys. **81**, 1773 (2009).

[25] R. Machleidt and D.R. Entem, Phys. Rep. **503**, 1 (2011).

[26] E. Epelbaum, A. Nogga, W. Glöckle, H. Kamada, Ulf-G. Meißner, and H. Witała, Phys. Rev. C **66**, 064001 (2002).

[27] A. Nogga, P. Navrátil, B. R. Barrett, and J. P. Vary, Phys. Rev. C **73**, 064002 (2006).

[28] P. Navrátil, Few Body Syst. **41**, 117 (2007).

[29] P. Navrátil, V. G. Gueorguiev, J. P. Vary, W. E. Ormand, and A. Nogga, Phys. Rev. Lett. **99**, 042501 (2007).

[30] R. Skibiński *et al.*, Phys. Rev. C **84**, 054005 (2011).

[31] N. Kalantar-Nayestanaki, E. Epelbaum, J.G. Messchendorp, and A. Nogga, Rep. Prog. Phys. **75**, 016301 (2012).

[32] F. Sammarruca, B. Chen, L. Coraggio, N. Itaco, and R. Machleidt, Phys. Rev. C **86**, 054317 (2012).

[33] M. Kohno, Phys. Rev. C **86**, 061301(R) (2012).

[34] A. Carbone, A. Polls, and A. Rios, Phys. Rev. C **88**, 044302 (2013).

[35] M. Kohno, Phys. Rev. C **88**, 064005 (2013).

[36] Th. A. Rijken and Y. Yamamoto, Phys. Rev. C **73**, 044008 (2006).

[37] Th. A. Rijken, Phys. Rev. C **73**, 044007 (2006).

[38] S. Rafi, M. Sharma, D. Pachouri, W. Haider, and Y. K. Gambhir, Phys. Rev. C **87**, 014003 (2013).

[39] R. B. Wiringa, V. G. J. Stoks, and R. Schiavilla, Phys. Rev. C **51**, 38 (1995).

[40] B. S. Pudliner, V. R. Pandharipande, J. Carlson, S. C. Pieper, and R. B. Wiringa, Phys. Rev. C **56**, 1720

(1997).

[41] B. Friedman and V. R. Pandharipande, Nucl. Phys. A **361**, 502 (1981).

[42] I. E. Lagaris and V. R. Pandharipande, Nucl. Phys. A **359**, 349 (1981).

[43] E. Epelbaum, W. Glöckle, and Ulf-G. Meißner, Nucl. Phys. A**747**, 362 (2005).

[44] K. Hebeler, S. K. Bogner, R. J. Furnstahl, A. Nogga, and A. Schwenk, Phys. Rev. C **83**, 031301(R) (2011).

[45] R. Machleidt, K. Holinde, and Ch. Elster, Phys. Rep. **149**, 1 (1987).

[46] T. Kasahara, Y. Akaishi, and H. Tanaka, Prog. Theor. Phys. Suppl. **56**, 96 (1974).

[47] B. A. Loiseau, Y. Nogami, and C. K. Ross, Nucl. Phys. A **165**, 601 (1971).

[48] J. W. Holt, N. Kaiser, and W. Weise, Phys. Rev. C **81**, 024002 (2010).

[49] J. W. Holt, N. Kaiser, G. A. Miller, and W. Weise, Phys. Rev. C **88**, 024614 (2013).

[50] M. I. Haftel and F. Tabakin, Nucl. Phys. A **158**, 1 (1970).

[51] K. Suzuki, R. Okamoto, M. Kohno, and S. Nagata, Nucl. Phys. A **665**, 92 (2000).

[52] D.R. Entem and R. Machleidt, Phys. Rev. **C68**, 041001 (2003).

[53] A. Noga, P. Navrátil, B.R. Barrett, and J.P. Vary, Phys.Rev. C73, 064002 (2006).

[54] J. W. Negele and D. Vautherin, Phys. Rev. C **5**, 1472 (1972).

[55] J. F. Berger, M. Girod, and D. Gogny, Comput. Phys. Commun. **63**, 365 (1991).

[56] T. Sumi *et al.*, Phys. Rev. C **85**, 064613 (2012).

[57] H. de Vries, C. W. de Jager, and C. de Vries, At. Data Nucl. Data Tables **36**, 495 (1987).

[58] R. P. Singhal, M. W. S. Macauley, and P. K. A. De Witt Huberts, Nucl. Instr. and Meth. **148**, 113 (1978).

[59] M. Ieiri *et al*., Nucl. Instr. and Meth. A **257**, 253 (1987).

[60] S. Kato *et al*., Phys. Rev. C **31**, 1616 (1985).

[61] H. Sakaguchi *et al*., Phys. Lett. B **89**, 40 (1979).

[62] H. Sakaguchi *et al*., Phys. Lett. B **99**, 92 (1981).

[63] E. L. Hjort *et al*., Phys. Rev. C **50**, 275 (1994).

[64] M. Baba *et al*., J. Nucl. Sci. Technol. Suppl. **2**, 204 (2002).

[65] A. Ingemarsson *et al*., Nucl. Phys. A **653**, 341 (1999).

[66] N. E. Davison *et al*., Nucl. Phys. A **290**, 45 (1977).

[67] J. J. H. Menet, E. E. Gross, J. J. Malanify, and A. Zucker, Phys. Rev. C **4**, 1114 (1971).

[68] K. Minomo, M. Toyokawa, M. Kohno and M. Yahiro, to be published in Phys. Rev. C:

arXiv:1404.5388 [nucl-th].